ROYAL SOCIETY
OF CHEMISTRY

PAPER

Check for updates

Single-atom transition metals doping two-dimensional B_XN materials (X = 2, 3, 5) with promising electrocatalytic activity for efficient hydrogen production in the entire pH range†

Yuhua Wei,[d] Feng Gao, [ID] *[abc] Hong Liu,[abc] Wei Qi,[bc] Sichao Du,[bc] Hao Xie[abc] and Duo Xiao[abc]

Two-dimensional (2D) boron nitrides (BN) have been eagerly and widely used and have tremendous potential in several advanced fields, such as energy harvesting and storage. Due to their significant electronic properties, they are also commonly used as substrates for single-atom catalysts (SACs). Therefore, with the aid of a computer, we designed SACs by doping isolated single atoms of 3d, 4d, and 5d transition metals (TM) on 2D B_XN materials (X = 2, 3, 5). In addition, pH regulation is considered to improve the electrocatalytic hydrogen evolution reaction (HER) activity, and the materials' effectiveness was investigated theoretically based on density functional theory (DFT) calculations. Our results indicate that the low-cost TM SACs can effectively enhance the HER catalytic performance over a wide range of pH. Among all the SACs studied, Ti-, V-, Y- and Zr@B_5N show excellent catalytic activity at pH = 0, with the Gibbs free energy change (ΔG_{H*}) of hydrogen adsorption of −0.027, −0.094, 0.073 and −0.040 eV, respectively. We find that Sc- and Y-embedded B_2N, Co-, Fe-, and Mo-embedded B_3N and Co-, Cr-, V-, Ti-, Y-, Zr-, Nb-, Ru-, and Tc-embedded B_5N SACs have excellent catalytic activity in acidic conditions, while Ir-embedded B_5N shows high catalytic activity in alkaline conditions. Interestingly, Ti@B_2N, Mn@B_3N, Fe@B_5N and Mo@B_5N SACs are highly active in either acidic or alkaline environments. Our work opens new avenues for designing cost-effective SACs with wide-pH-range HER performance.

1. Introduction

Hydrogen is considered to become the cleanest energy source in the world due to its advantages such as abundant raw materials, environmental protection, high energy and recyclability.[1–3] Therefore, the development of a safe, efficient and low-cost hydrogen production process is crucial to solve the serious environmental pollution and energy shortage problems. Among them, electrochemical hydrogen evolution reaction (HER) is considered to be the most promising and sustainable industrial hydrogen production method, and the role of catalysts is indispensable.[4–8] At present, the precious

metal platinum is considered to be the best electrocatalyst for HER because of its excellent kinetic and thermodynamic efficiency.[9–13] However, the scarcity and high cost of precious metals are important factors hindering their large-scale and sustainable application, which cannot be ignored.[13–15] Therefore, it is very important to find both efficient and low-cost HER electrocatalysts, which have extremely important significance.

In order to develop a practical HER catalyst—in addition to considering some basic requirements such as the cost, stability and conductivity of the catalyst—it must also have the ability to trigger proton reduction with the minimum overpotential, as well as fast kinetic performance. In recent years, the unique surface structure and electronic properties of two-dimensional (2D) materials have provided new opportunities and challenges in the development of HER catalysts.[16–23] Two-dimensional materials have the advantages of high durability, low cost and excellent environmental protection, and they have unique physical and chemical properties such as stronger surface activity, faster charge transfer and adjustable band gap, which give them broad application potential in the fields of catalysts, sensors and photodetectors.[24–33] So far, 2D HER catalysts based on non-metallic nanomaterials have received a lot of attention.

a School of Information and Electrical Engineering, Hangzhou City University, Hangzhou, Zhejiang 310015, China. E-mail: gaofengphys@163.com

b Academy of Edge Intelligence Hangzhou City University, Hangzhou City University, Hangzhou, Zhejiang 310015, China

c Zhejiang Engineering Research Center for Edge Intelligence Technology and Equipment, Hangzhou City University, Hangzhou, Zhejiang 310015, China

d Department of Physics, International Centre of Quantum and Molecular Structures, Shanghai University, Shanghai 200444, China

† Electronic supplementary information (ESI) available. See DOI: https://doi.org/10.1039/d4ma00161c

The intrinsic catalytic activity of 2D materials and the formation of single atom catalysts (SACs) by deposition of transition metal (TM) atoms on the surface of 2D materials are two new areas of cutting-edge catalytic research, which have revealed new catalytic processes at the atomic scale.[34–36]

In recent studies, various synthesized SACs showed excellent catalytic properties in different reactions.[37–40] In order to meet the basic requirements of efficient SAC substrate materials, it is necessary to select a low-cost and highly stable substrate material, which should have abundant metal and good electrical conductivity, as well as a large specific surface area and multiple active centers. Among the many 2D materials, materials with metallic properties are a good choice. However, due to the wide variety of 2D materials, sifting through thousands of candidates remains a major challenge. The process of screening hydrogen evolution electrocatalysts can be greatly accelerated by using descriptors based on catalytic performance and density functional theory (DFT) calculations.[41–43] To address the current challenges in the screening of 2D materials as SAC substrate materials, we designed a study to focus on the possibility of anchoring transition metal atoms in novel 2D substrate materials, and here we explore and report on the importance of such SAC descriptors. Recently, through first-principles swarm intelligence structure calculations, several 2D B_XN materials (X = 2, 3, 5) have been successfully discovered. These B_XN materials have high cohesion energy and good kinetic, thermodynamic and mechanical stability, making them highly feasible for experimental synthesis.[44] B_XN materials also exhibit excellent recyclability and improved metal conductivity after TM loading, showing great potential for hydrogen evolution SAC applications.

In this work, based on first principles, we studied the catalytic activity in HER of TM single atoms loaded on B_XN materials' surface, and discuss the mechanism of the high catalytic activity of the SCAs. Zhou et al. have verified the structural stability of 2D B_XN materials through phonon spectrum calculation and ab initio molecular dynamics simulation (AIMD).[44] We studied a variety of transition metal elements, including the 3d, 4d, and 5d groups. Here, the catalytic activity of SACs in HER is described by the Gibbs free energy change (G_{H^*}) of hydrogen adsorption. The descriptors proposed in this paper only include some inherent properties of substrate materials and provide a simple and rapid method for designing and screening HER electrocatalysts more effectively. Additionally, the optimal HER activity of 2D B_XN catalysts in all pH ranges was investigated. Ti-, V-, Y- and Zr-embedded B_5N SACs have high HER activity with moderate and good electrical conductivity before and after H binding at pH = 0. In addition, the 3d-B_2N, 3d-B_3N, 3d-B_5N and 4d-B_5N SACs studied have high activity over a wide pH range. Specifically, 3d-B_2N and 3d-B_3N SACs are suitable for acidic environments, and 4d-B_5N SACs are suitable for alkaline environments, because the electron state near the Fermi level increases and the charge density on the surface increases. The high concentration of free charges is a key factor in HER progression.

2. Computational methods

All spin-polarized calculations in this section were performed by using the vienna ab initio simulation package (VASP)[45,46] based on density functional theory. The generalized gradient approximation (GGA)[47] of the Perdew–Burke–Ernzerhof (PEB)[48] functional was used to describe the exchange correlation energy, and the projection plane-wave (PAW) method[49] was used to describe the pseudopotential of all atoms. In order to eliminate the influence of van der Waals (vdW) forces, Grimme's empirical correction method, namely, DFT+D3,[50,51] was used in structural optimizations and property calculations of the 2D B_XN materials. A cutoff energy of 500 eV for the plane-wave basis was adopted. The energy and force convergence criteria for self-consistent optimizations were set to 10^{-5} eV and 10^{-3} eV Å^{-1}, respectively. In the process of structural optimization, the inverted vector k-point grids of 2D B_XN materials were divided into $2\pi \times 0.03$ Å^{-1}. It is worth mentioning that when calculating electronic properties, the inverted lattice vector k-point grid for all structures in the self-consistent iteration process was set to a larger value. A $2 \times 2 \times 1$ monolayer of 2D B_XN materials was adapted for all calculations, and a vacuum space of 20 Å along the z direction was included to prevent interactions between periodic images. In ab initio molecular dynamics (AIMD) simulations, integration of the equations of motion proceeded with time steps of 1.0 fs for different temperature ranges.[52] Typical simulations ran for 3000 steps with the time scale of about 3 ps. The isokinetic ensemble (NVT) was employed for the ions, where the ion temperature T_i was fixed using velocity scaling. As is well known, the influence of the solvation effect on the process of hydrogen adsorption is so slight that the solvation effect can be omitted, so we will not consider the calculations of solvation effect in this work.[52–55] For more computational details, please see the ESI.†

3. Results and discussion

According to previous reports, the B_2N, B_3N and B_5N structures were constructed in diverse orthorhombic configuration with the space group of AMM2, AMM2 and PMC21, respectively.[44] Fig. 1(a)–(c) illustrate the schematic diagrams of the 2D B_XN materials (X = 2, 3, 5), which are composed of three different unit cells, respectively. The common feature is the presence of a five-member ring or even a six-member ring formed by boron atoms crossing with the nitrogen atoms in all the 2D B_XN materials' unit cells. The optimized lattice constant of 2D B_XN materials is calculated to be a = 10.29 Å, b = 3.91 Å (X = 2); a = 10.13 Å, b = 4.80 Å (X = 3); and a = 6.41 Å, b = 2.69 Å (X = 5), respectively, in good accordance with previous studies.[44] In order to explore the TM adsorption behavior on the surface of 2D B_XN materials, a 2×2 supercell containing 72 atoms, 2×2 supercell including 64 atoms and 2×2 supercell involving 48 atoms as the substrate for the adsorption were constructed, correspondingly. Dynamic stability is an inevitable index in material design. So, in order to evaluate the dynamic stability of the B_XN materials, we calculated their phonon
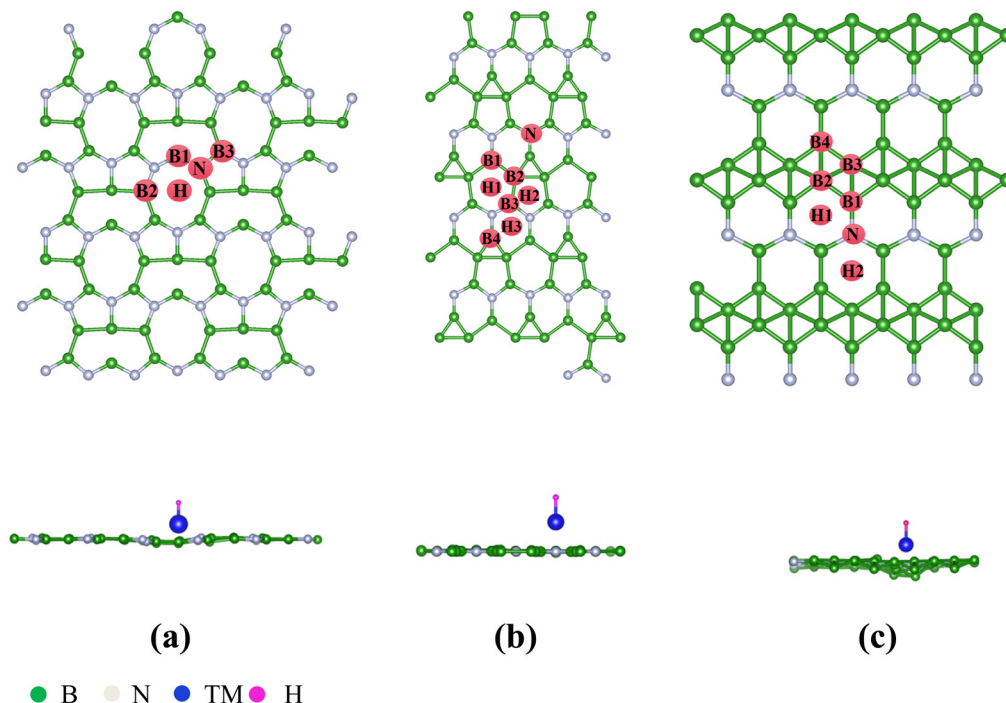
Fig. 1 Top and side views of the optimized structures of the 2D B_XN materials: (a) B_2N monolayer, (b) B_3N monolayer, and (c) B_5N monolayer with the TM and H being adsorbed at the optimal HER sites.

spectra. As shown in Fig. S1 (ESI†), no negative frequency is observed in the entire Brillouin region, indicating that the B_2N, B_3N and B_5N monolayers have good dynamic stability. Three different sites are considered for TM adsorption on the B_XN materials, including the hollow of the surface B–N ring, the top site of B atom and the top site of surface N atom. Then, binding energy (E_b) calculations were implemented to evaluate the stability and feasibility of experimental synthesis of SACs for each configuration based on eqn (S1) (ESI†). Isolated Sc, as the test atom, adsorbs on nine different configurations, and the E_b was calculated between the Sc atom and substrates. Finally, it can be found from Table S1 (ESI†) that among the adsorption configurations, Sc adsorption on the hollow of 2D B_XN material (X = 2, 3, 5) surface is the most energetically favorable, with the E_b of −4.75 eV, −3.91 eV and −5.18 eV, respectively. Then, the use of 2D B_XN materials as substrates to anchor single atoms of 3d, 4d, and 5d TM was further investigated, and the E_b between TM atom and B_XN materials was calculated. The corresponding E_b, cohesive energies (E_{coh}) and the energy difference (ΔE) between E_b and E_{coh} of all TM@B_XN materials studied in the present work are shown in Fig. 2 and Fig. S2, S3 (ESI†). The E_{coh} can be calculated by the following equation:

$$E_{coh} = (E_{M(bulk)})/n \quad (1)$$

where $E_{M(bulk)}$ is the energy of M crystals and n is the number of M atoms in the unit cell of crystals, and these values were compared with the adsorption energies. Because the energy advantage of TM clusters is essentially lower than that of metal crystals, to avoid the formation of clusters among TM atoms, we set a standard for judging system stability, that is,
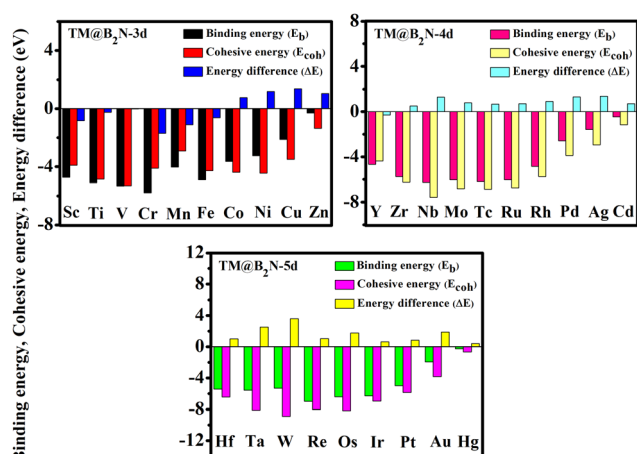

Fig. 2 . Adsorption of different TM atoms on the B_2N monolayer and the corresponding binding energy (E_b), cohesive energy (E_{coh}) and their energy difference (ΔE).

ΔE < 0 eV. As indicated in Fig. 2, the ΔE values are positive for all 5d-TM@B_2N systems, and only six TM atoms of 3d state (Fe, Mn, Ti, V, Cr and Sc) and one TM atom of 4d state (Y) can immobilize on the B_2N materials with ΔE < 0 eV. Similarly, the calculated ΔE values are positive for all 5d-TM@B_3N systems, and only Co, Fe, Cr, Mn and Mo atoms can adsorb stably on B_3N materials. For the B_5N system, it is obvious that the adsorption of TM atoms by B_5N materials is stronger than that by B_2N and B_3N materials. Most TM atoms, such as Co, Fe, Mn, Ti, V, Cr, Sc, Y, Zr, Nb, Mo, Tc, Ru and Ir, including the 3d, 4d and 5d groups, are effectively adsorbed on the B_5N materials.

expressed by Volmer–Tafel and Volmer–Heyrovsky reaction pathways. The two reaction equations are divided into three key steps:

$$\text{Volmer step: } H^+ + e^- + * \rightarrow H* \qquad (2)$$

$$\text{Heyrovsky step: } H* + H^+ + e^- \rightarrow H_{2+}* \qquad (3)$$

$$\text{Tafel step: } H* + H* \rightarrow H_2 + 2* \qquad (4)$$
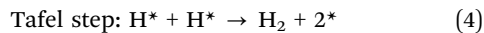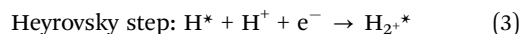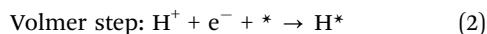
where $*$ and $H*$ represent the active site on the catalyst surface and the intermediate hydrogen adsorbed on the surface, respectively. For the Heyrovsky reaction, H_2 is generated when adsorbed hydrogen ($H*$) interacts with H_3O^+ clusters. As shown in Fig. S7 (ESI†), the calculated energy barrier for the Heyrovsky pathway of the Ti@B$_5$N monolayer is 1.78 eV, while the activation energy barrier of the Tafel reaction of the Ti@B$_5$N monolayer is 0.52 eV. Thus, the HER mechanism of the Ti@B$_5$N monolayer may follow the Tafel-dominated Volmer–Tafel reaction. Similarly, the HER mechanism of the V@B$_5$N monolayer also follows the Volmer–Tafel reaction. Nevertheless, under alkaline conditions, water dissociation produces hydrogen ions (H^+), and the two important reaction steps are given as follows:

$$\text{Alkaline Volmer step: } H_2O + e^- + * \rightarrow H* + OH^- \qquad (5)$$

$$\text{Alkaline Heyrovsky step: } H* + H_2O + e^- \rightarrow H_2 + OH^- + * \qquad (6)$$
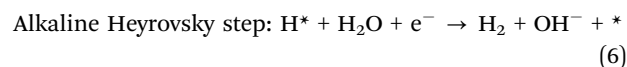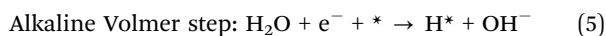
Under alkaline conditions, the apparent HER activity is limited by hydrolytic dissociation, which produces $H*$ and is sensitive to pH, so the energy barrier of hydrolytic dissociation needs to be considered. At the same time, more and more computational and experimental studies have proven that the hydrolytic separation energy barrier plays an important role in the alkaline hydrogen evolution process. As shown in Fig. S8 (ESI†), it is found through calculation that Ti- and V-modified B$_5$N have rapid hydrolysis dissociation ability, with the energy barrier of about 0.23 and 0.09 eV, which can realize rapid proton transfer. Therefore, Ti, V and BS-B1P1 can cooperate well to accelerate alkaline HER.

Fig. 4 shows the ΔG_{H*} for single H atom adsorption on TM@B$_X$N systems at pH = 0. Ti@B$_5$N, V@B$_5$N, Y@B$_5$N and Zr@B$_5$N SACs show excellent catalytic activity with ΔG_{H*} values of −0.027, −0.094, 0.073 and −0.04 eV, respectively. It can be seen that the ΔG_{H*} of these SACs are even low as ∼ −0.027 eV, superior to precious metals such as Pt. In reality, electrocatalysts need to undergo charge adjustment to match their Fermi level with the applied electrode potential, and therefore, a grand-canonical ensemble of electrons under the constant
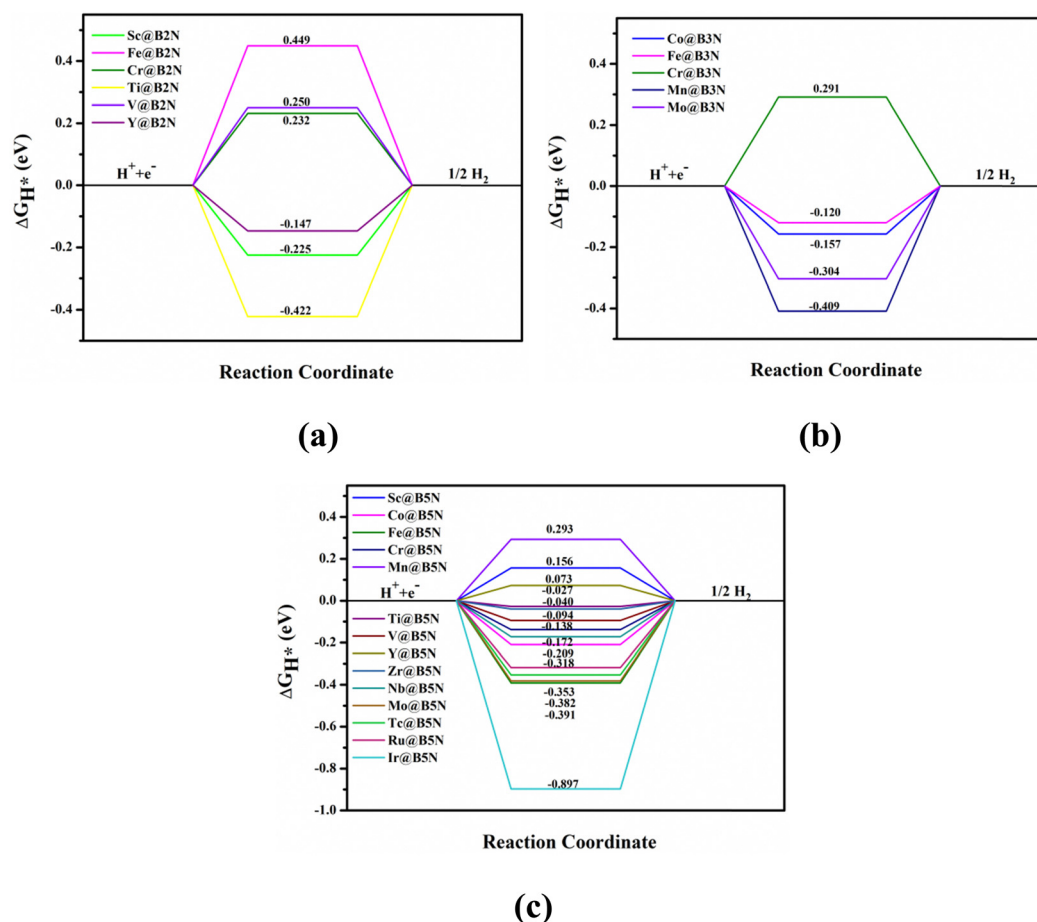

Fig. 4 Free energy diagram for HER of different TM atoms on the (a) B$_2$N, (b) B$_3$N, and (c) B$_5$N monolayer compounds under standard conditions.
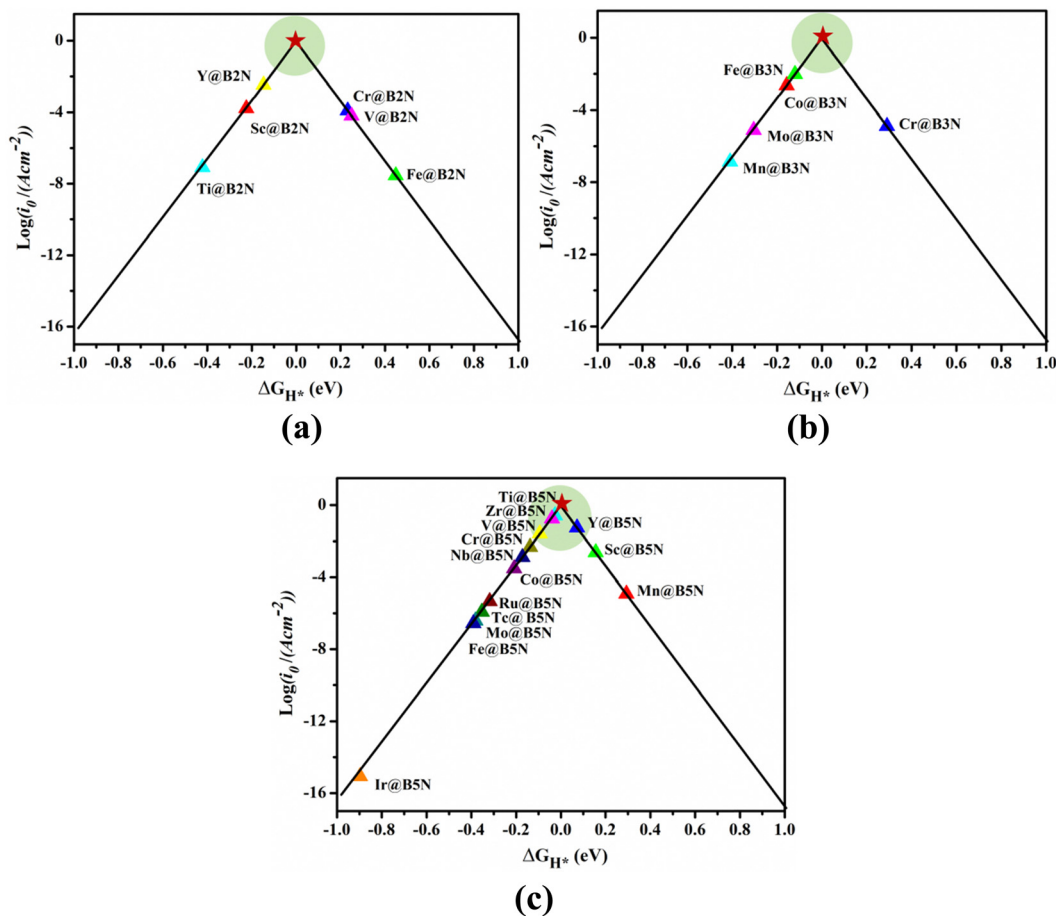
Fig. 5 HER volcano curve of exchange current (i_0) as a function of the Gibbs free energy change (ΔG_{H^*}) of hydrogen adsorption on (a) TM@B$_2$N, (b) TM@B$_3$N, and (c) TM@B$_5$N systems.

potential model (CPM) is better at reflecting practical electro-catalytic conditions.[63,64] We supplemented the calculation of ΔG_{H^*} corresponding to different potentials under the CPM model. According to Fig. S9 (ESI†), it can be clearly found that TM@B$_5$N SACs with good catalytic performance show little change in ΔG_{H^*} at different potentials, and still have excellent catalytic performance. In addition, TM@B$_5$N SACs have the best HER catalytic active sites on the hollow of the 2D B$_5$N surface. Nevertheless, the decoration of TM atoms can reinforce well the binding of H atoms to the B$_2$N and B$_3$N materials, but it performs poorly in enhancing the HER catalytic activity of the TM@B$_2$N and TM@B$_3$N SACs, showing inferior ΔG_{H^*} values. This means that at pH = 0, low-cost TM@B$_5$N SACs may become substitutes for precious metal catalysts to improve the performance of HER. To more intuitively compare the catalytic activity of TM@B$_X$N SACs at pH = 0, the corresponding volcano curves are plotted in Fig. 5. According to Norskov's hypothesis, where a simple kinetic model is established to understand the origin of the volcano, the exchange current density (i_0) based on ΔG_{H^*} was studied and calculated.[65] When $\Delta G_{H^*} < 0$, the expression of exchange current is expressed as:

$$i_0 = -ek_0\frac{1}{1 + \exp(-\Delta G_{H^*}/k_B T)} \quad (7)$$

when $\Delta G_{H^*} > 0$, the exchange current is:

$$i_0 = -ek_0\frac{1}{1 + \exp(\Delta G_{H^*}/k_B T)} \quad (8)$$

where k_0 is the rate constant and k_B is the Boltzmann constant. Because there are no experimental data available, k_0 is set to 1.[66] First, the volcano map is drawn with ΔG_{H^*} as the horizontal coordinate and i_0 as the vertical coordinate. The HER catalytic activity of these SACs can be better observed based on the position of ΔG_{H^*} and i_0 relative to the volcanic peak, where the closer the location is to the volcanic peak, the higher the HER activity of the SACs. As shown in Fig. 5(c), Ti@B$_5$N, V@B$_5$N, Y@B$_5$N and Zr@B$_5$N systems achieve the maximum exchange current rates on account of the appropriate interactions between TM (Ti, V, Y, Zr) and H atoms, implying a promising catalytic activity for HER. However, most TM@B$_2$N SACs, such as Co@B$_5$N, Cr@B$_5$N, Fe@B$_5$N, Nb@B$_5$N, Ru@B$_5$N, Tc@B$_5$N, Mo@B$_5$N and Ir@B$_5$N, exhibit poor HER performance due to the strong bonding strength between H atoms and TM atoms, and are mainly distributed on the left side of the volcano map. Sc@B$_5$N and Mn@B$_5$N SACs are on the right side of the volcano map because of the weak interaction between H and TM atoms, which results in positive ΔG_{H^*} values. However, among the

pre-screened TM@B$_2$N (TM = Sc, Cr, V, Ti, Fe and Y) and TM@B$_3$N (TM = Co, Cr, Fe, Mn and Mo) SACs (shown in Fig. 5(a) and (b)), Ti-, Mn-, and Y@B$_2$N; and Co-, Fe-, Mn-, Mo@B$_3$N are mainly distributed on the left side of the volcano diagram, showing strong hydrogen adsorption, to the disadvantage of the release of atomic hydrogen. V-, Fe-, Cr@B$_2$N and Cr@B$_3$N SACs are on the right side of the volcano curve with highly positive ΔG_{H*} values, which is not conducive to the adsorption of atomic hydrogen on the TM atom, thus exhibiting low i_0 values. It is obvious that most SACs have negative ΔG_{H*} values because of the strong adsorption between hydrogen atoms and TM atoms. However, pH modification can effectively improve the catalytic activity of these SACs, so as to have a suitable ΔG_{H*} value. In neutral or alkaline environment, water molecules (H$_2$O) are first adsorbed and decomposed on the SAC surface (Volmer process: H$_2$O + e$^-$ + * → H* + OH$^-$). Then, two adjacent adsorbed hydrogen atoms on the SAC surface will combine to form a molecule of hydrogen (Heyrovsky process: H* + H$_2$O + e$^-$ → H$_2$ + OH$^-$ + *). SACs in this process promote the formation of hydrogen molecules.

We can regard the effect of pH on ΔG_{H*} as an additional entropic potential. Then the pH-dependent ΔG(pH) can be obtained by eqn (S7) (ESI†): ΔG(pH) = $k_B T$ln(10) × pH, which is conducive to understanding the relationship between HER performance and pH. Fig. 6(a)–(d) show the effect of different

pH on the HER performance of all pre-screened SACs, including 3d-, 4d and 5d-TM@B$_x$N systems. It is obvious that as the pH value is increased from 1 to 14, ΔG_{H*} value gradually increases, meaning that the adsorption inclination between hydrogen atom and SACs significantly decreases. By exploring the dependence of H adsorption on different SACs with pH, the optimal SACs for HER can be found. Fig. 6(c and d) show the linear relationship between the pH and ΔG_{H*} of TM@B$_5$N SACs. Fig. 6(c) indicates that for 3d-TM@B$_5$N SACs, only V@B$_5$N and Ti@B$_5$N systems lie in the optimal HER activity range at pH = 0. With increasing pH from 0 to 3, HER activity of the V@B$_5$N and Ti@B$_5$N SACs decreases, ΔG_{H*} increases from −0.027 to 0.100 eV, indicating that V@B$_5$N and Ti@B$_5$N SACs can maintain ultra-high HER activity in a strong acid environment. Cr@B$_5$N and Co@B$_5$N SACs can only have excellent catalytic activity in strong acid or weak acid environment, with pH regulation from 2 to 6. It is worth mentioning that Fe@B$_5$N SAC can effectively catalyze HER under weak acid, neutral and alkaline conditions, which means that Fe@B$_5$N SAC has a wide range of choices in different pH environments. Fig. 6(d) gives the ΔG_{H*} vs. pH for the 4d and 5d-TM@B$_5$N SACs. Compared with 3d-TM@B$_5$N SACs, the effect of pH on 4d and 5d-TM@B$_5$N SACs is more obvious, which is reflected in their obvious increase of catalyst activity in the pH range from 0 to 14. As can be seen from the figure at pH = 0, the adsorption between 4d,
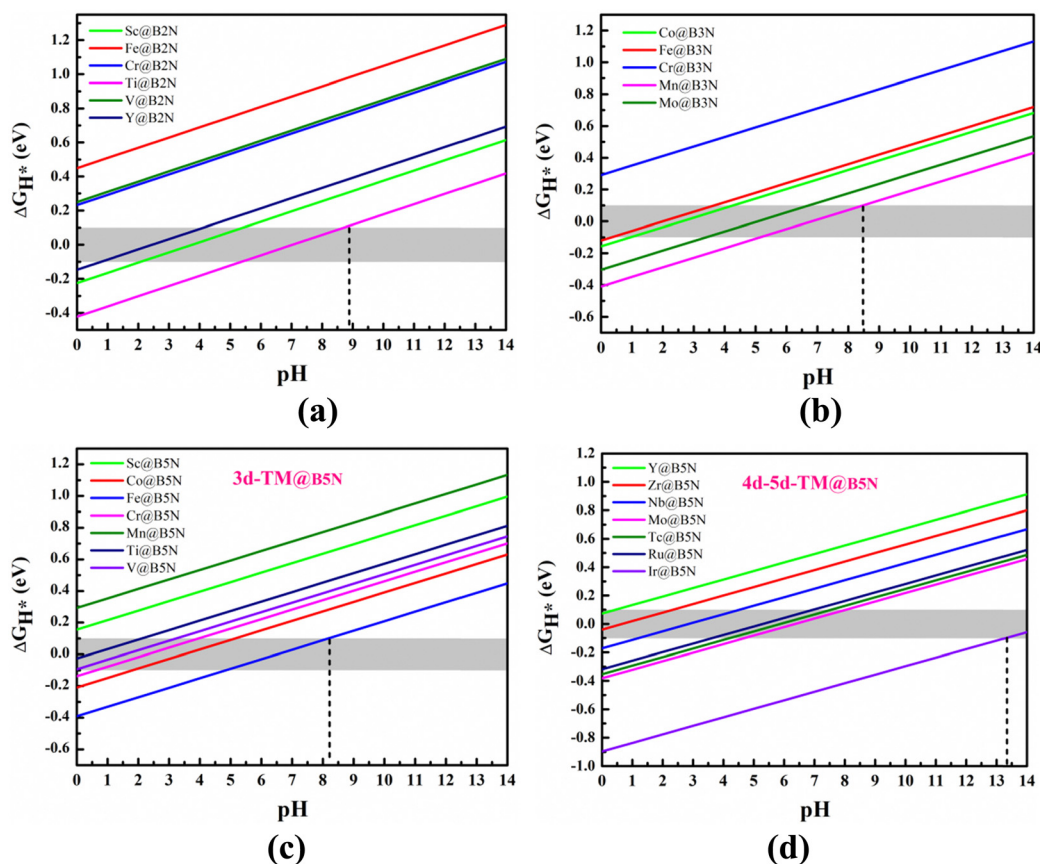

Fig. 6 The pH dependence of H-adsorption free energy of TM atom adsorption on the (a) B$_2$N, (b) B$_3$N and (c) and (d) B$_5$N monolayer compounds. The pink shaded area in the figures indicates the ideal ΔG_{H*} value range.

5d TM atoms and H atom is too strong, leading to a more negative ΔG_{H^*}. As pH increases, the bonding strength between 4d, 5d TM atoms and the H atom is further weakened, bringing ΔG_{H^*} down to a suitable value. In the pH range of 0 to 2.5, that is, under strong acid conditions, Y@B$_5$N and Zr@B$_5$N SACs are highly active in HER. In contrast, Ir@B$_5$N SAC has good catalytic activity in a strong alkali environment. Nb@B$_5$N SAC can maintain excellent HER activity under a stronger acid environment with pH range of 2 to 4.5, while only under the condition of weak acid with pH range of 4 to 7 can Ru@B$_5$N and Tc@B$_5$N SACs effectively catalyze HER. Similar to Fe@B$_5$N SAC, Mo@B$_5$N SAC can also play a catalytic role under weak acid, neutral and alkaline conditions. The variation of ΔG_{H^*} with pH of TM@B$_2$N SACs is shown in Fig. 6(a). It is obvious that TM@B$_2$N SACs mainly promote HER under acidic conditions. For example, Sc@B$_2$N and Y@B$_2$N SACs are active under the weak-acid or strong-acid condition with pH range of 1 to 5.5, and the HER performance of Ti@B$_2$N SAC can be greatly improved in either acidic, neutral or alkaline conditions with pH range of 5.5 to 9. As seen in Fig. 6(b), TM@B$_3$N SACs also catalyze the conversion process from atomic H to H$_2$ mainly under acidic conditions. Fe@B$_3$N and Co@B$_3$N SACs have excellent catalytic activity in strong acid environment with pH regulation from 1 to 4. Mo@B$_3$N SAC shows stronger HER catalysis in the weak acid environment, with the pH range of 4 to 7. Interestingly, Mn@B$_3$N SAC can be effectively adjusted by pH and gives weak acid, neutral and alkaline HER activity within the pH range of 5 to 8.5. In short, our results suggest that the HER activity of TM@B$_X$N SACs is closely associated with pH. The TM@B$_X$N SACs are not only catalytically active in acidic conditions but also exhibit high HER catalytic activity in alkaline environments. Remarkably, Ti@B$_2$N, Mn@B$_3$N, Fe@B$_5$N and Mo@B$_5$N SACs have potential to be a multifunctional catalyst with a wide pH threshold.

4. Conclusions

In summary, we designed promising SACs composed of 3d-, 4d-, and 5d-TM atoms and 2D B$_X$N materials toward efficient HER using first-principles calculations. Some stable TM@B$_X$N SACs were screened by theoretical calculations, and DOS calculations show that these SACs have good electrical conductivity, providing favorable conditions for rapid transfer among electrons. In addition, free energy calculations showed that the TM@B$_X$N SACs exhibit different catalytic performance in different pH ranges. Ti-, V-, Y- and Zr-embedded B$_5$N SACs have high HER activity with moderate and good electrical conductivity before and after H binding at pH = 0. TM@B$_2$N and TM@B$_3$N SACs have excellent HER performance in acid environment. Remarkably, three different TM@B$_X$N systems have appropriate SACs which can maintain high HER catalytic activity in acidic, neutral and alkaline environments to promote the conversion of atomic H to H$_2$. Therefore, our works demonstrate that the cost-effective TM@B$_X$N can serve as SACs to facilitate HER, which provides a theoretical reference for future application in practice.

Data availability

All data generated or analyzed during this study are included in this published article and its ESI† files.

Conflicts of interest

The authors report no conflicts of interest. The authors alone are responsible for the content and writing of the paper.

Acknowledgements

References

1 K. Mazloomi and C. Gomes, Hydrogen as an energy carrier: Prospects and challenges, *Renewable Sustainable Energy Rev.*, 2012, **16**, 3024–3033.

2 J. Luo, J.-H. Im, M. T. Mayer, M. Schreier, M. K. Nazeeruddin and N.-G. Park, *et al.*, Water photolysis at 12.3% efficiency via perovskite photovoltaics and Earthabundant catalysts, *Science*, 2014, **345**, 1593–1596.

3 S. Z. Baykara, Hydrogen: a brief overview on its sources, production and environmental impact, *Int. J. Hydrogen Energy*, 2018, **43**, 10605–10614.

4 M. S. Dresselhaus and I. L. Thomas, Alternative energy technologies, *Nature*, 2001, **414**, 332–337.

5 S. Chu and A. Majumdar, Opportunities and challenges for a sustainable energy future, *Nature*, 2012, **488**, 294–303.

6 Y. Zheng, Y. Jiao, Y. Zhu, L. Li, Y. Han, Y. Chen, A. Du, M. Jaroniec and S. Qiao, Hydrogen evolution by a metal-free electrocatalyst, *Nat. Commun.*, 2014, **5**, 3783.

7 J. Mahmood, F. Li, S.-M. Jung, M. S. Okyay, I. Ahmad, S.-J. Kim, N. Park, H. Y. Jeong and J.-B. Baek, An efficient and pH-universal ruthenium-based catalyst for the hydrogen evolution reaction, *Nat. Nanotechnol.*, 2017, **12**, 441–446.

8 G. Zhao, K. Rui, S. X. Dou and W. Sun, Heterostructures for electrochemical hydrogen evolution reaction: a review, *Adv. Funct. Mater.*, 2018, **28**, 1803291.

9 D. V. Esposito, S. T. Hunt, A. L. Stottlemyer, K. D. Dobson, B. E. McCandless, R. W. Birkmire and J. G. Chen, Low-cost hydrogen-evolution catalysts based on monolayer platinum on tungsten monocarbide substrates, *Angew. Chem., Int. Ed.*, 2010, **49**, 9859–9862.

10 L. A. Kibler, Hydrogen Electrocatalysis, *ChemPhysChem*, 2006, **7**, 985–991.

11 Y.-J. Wang, N. Zhao, B. Fang, H. Li, X. T. Bi and H. Wang, Carbon-supported Pt-based alloy electrocatalysts for the oxygen reduction reaction in polymer electrolyte membrane fuel cells: particle size, shape, and composition manipulation and their impact to activity, *Chem. Rev.*, 2015, **115**, 3433–3467.

12 R. Subbaraman, D. Tripkovic, D. Strmcnik, K. C. Chang, M. Uchimura, A. P. Paulikas, V. Stamenkovic and N. M. Markovic, Enhancing Hydrogen Evolution Activity in Water Splitting by Tailoring Li^+-$Ni(OH)_2$-Pt Interfaces, *Science*, 2011, **334**, 1256–1260.

13 Y. Zheng, Y. Jiao, M. Jaroniec and S. Z. Qiao, Advancing the Electrochemistry of the Hydrogen-Evolution Reaction through Combining Experiment and Theory, *Angew. Chem., Int. Ed.*, 2015, **54**, 52–65.

14 H. Xu, D. Cheng, D. Cao and X. C. Zeng, A universal principle for a rational design of single-atom electrocatalysts, *Nat. Catal.*, 2018, **1**, 339–348.

15 X. Liu and L. Dai, Erratum: Carbon-based metal-free catalysts, *Nat. Rev. Mater.*, 2016, **1**, 16064.

16 X. Lv, W. Wei, Q. Sun, F. Li, B. Huang and Y. Dai, Two-dimensional germanium monochalcogenides for photocatalytic water splitting with high carrier mobility, *Appl. Catal., B*, 2017, **217**, 275–284.

17 T. Liao, L. Kou, A. Du, Y. Gu and Z. Sun, Simplest MOF units for effective photodriven hydrogen evolution reaction, *J. Am. Chem. Soc.*, 2018, **140**, 9159–9166.

18 C. Liu, Q. Li, C. Wu, J. Zhang, Y. Jin, D. R. MacFarlane and C. Sun, Single-boron catalysts for nitrogen reduction reaction, *J. Am. Chem. Soc.*, 2019, **141**, 2884–2888.

19 L. X. Chen, Z. W. Chen, Y. Wang, C. C. Yang and Q. Jiang, Design of dual-modified MoS_2 with nanoporous Ni and graphene as efficient catalysts for the hydrogen evolution reaction, *ACS Catal.*, 2018, **8**, 8107–8114.

20 G. Gao, Y. Jiao, E. R. Waclawik and A. Du, Single atom (Pd/Pt) supported on graphitic carbon nitride as an efficient photocatalyst for visible-light reduction of carbon dioxide, *J. Am. Chem. Soc.*, 2016, **138**, 6292–6297.

21 F. Gao, Y. H. Wei, J. G. Du and G. Jiang, Theoretical screening of 2D materials supported transition-metal single atoms as efficient electrocatalysts for hydrogen evolution reaction, *Materialia*, 2021, **18**, 101168.

22 Y. H. Wei, F. Gao, J. G. Du and G. Jiang, Modulation of the B_4N monolayer as an efficient electrocatalyst for hydrogen evolution reaction, *Int. J. Hydrogen Energy*, 2022, **47**, 11511–11519.

23 Y. H. Wei, F. Gao, H. C. Huang and G. Jiang, Two-dimensional B_7P_2: Dual-purpose functional material for hydrogen evolution reaction/hydrogen storage, *Int. J. Hydrogen Energy*, 2022, **47**, 8338–8347.

24 Z. Zhang, Y. Yang, G. Gao and B. I. Yakobson, Two-Dimensional Boron Monolayers Mediated by Metal Substrates, *Angew. Chem., Int. Ed.*, 2015, **54**, 13022–13026.

25 G. R. Bhimanapati, Z. Lin, V. Meunier, Y. Jung and J. Cha, Recent Advances in Two-Dimensional Materials beyond Graphene, *ACS Nano*, 2015, **9**, 11509–11539.

26 S. Zhang, W. Zhou, Y. Ma, J. Ji, B. Cai, S. A. Yang, Z. Zhu, Z. Chen and H. Zeng, Antimonene Oxides: Emerging Tunable Direct Bandgap Semiconductor and Novel Topological Insulator, *Nano Lett.*, 2017, **17**, 3434–3440.

27 S. Milana, The Lab-to-Fab Journey of 2D Materials, *Nat. Nanotechnol.*, 2019, **14**, 919–921.

28 H. Shu, D. Zhou, F. Li, D. Cao and X. Chen, Defect Engineering in $MoSe_2$ for the Hydrogen Evolution Reaction: From Point Defects to Edges, *ACS Appl. Mater. Interfaces*, 2017, **9**, 42688–42698.

29 M. Zeng, Y. Chen, J. Li, H. Xue, R. G. Mendes, J. Liu, T. Zhang, M. H. Rümmeli and L. Fu, 2D WC Single Crystal Embedded in Graphene for Enhancing Hydrogen Evolution Reaction, *Nano Energy*, 2017, **33**, 356–362.

30 P. Manchanda, A. Enders, D. J. Sellmyer and R. Skomski, Hydrogen-Induced Ferromagnetism in Two-Dimensional Pt Dichalcogenides, *Phys. Rev. B*, 2016, **94**, 104426.

31 S. Lei, X. Wang, B. Li, J. Kang, Y. He, A. George, L. Ge and Y. Gong, Surface Functionalization of Two Dimensional Metal Chalcogenides by Lewis Acid-Base Chemistry, *Nat. Nanotechnol.*, 2016, **11**, 465–471.

32 D. Akinwande, C. J. Brennan, J. S. Bunch, P. Egberts, J. R. Felts and H. Gao, A Review on Mechanics and Mechanical Properties of 2D Materials Graphene and Beyond, *Extreme Mech. Lett.*, 2017, **13**, 42–77.

33 C. Tan, C. Cao, X.-J. Wu, Q. He, J. Yang, X. Zhang, J. Chen, W. Zhao and S. Han, Recent Advances in Ultrathin Two-Dimensional Nanomaterials, *Chem. Rev.*, 2017, **117**, 6225–6331.

34 X.-F. Yang, A. Wang, B. Qiao, J. Li, J. Liu and T. Zhang, Single-atom catalysts: a new frontier in heterogeneous catalysis, *Acc. Chem. Res.*, 2013, **46**, 1740–1748.

35 H. Fei, J. Dong, Y. Feng, C. S. Allen, C. Wan and B. Volosskiy, General synthesis and definitive structural identification of MN_4C_4 single-atom catalysts with tunable electrocatalytic activities, *Nat. Catal.*, 2018, **1**, 63–72.

36 C. Ling, X. Bai, Y. Ouyang, A. Du and J. Wang, Single molybdenum atom anchored on N-doped carbon as a promising electrocatalyst for nitrogen reduction into ammonia at ambient conditions, *J. Phys. Chem. C*, 2018, **122**, 16842–16847.

37 J. Su, R. Ge, Y. Dong, F. Hao and L. Chen, Recent progress in single-atom electrocatalysts: concept, synthesis, and applications in clean energy conversion, *J. Mater. Chem. A*, 2018, **6**, 14025–14042.

38 X. Su, X. F. Yang, Y. Huang, B. Liu and T. Zhang, Single-Atom Catalysis toward Efficient CO_2 Conversion to CO and Formate Products, *Acc. Chem. Res.*, 2019, **52**, 656–664.

39 R. Zhang, L. Jiao, W. Yang, G. Wan and H. L. Jiang, Single-atom catalysts templated by metal–organic frameworks for electrochemical nitrogen reduction, *J. Mater. Chem. A*, 2019, **7**, 26371–26377.

40 X. Zhang, Z. Zhang, D. Wu, X. Zhang, X. Zhao and Z. Zhou, Computational screening of 2D materials and rational design of heterojunctions for water splitting photocatalysts, *Small Methods*, 2018, **2**, 1700359.

41 Z. H. Zhang, X. Zhang, X. D. Zhao, S. Yao, A. Chen and Z. Zhou, Algorithm screening to accelerate discovery of 2D

metal-free electrocatalysts for hydrogen evolution reaction, *ACS Omega*, 2019, **4**, 7822–7828.

42 S. Yao, X. Zhang and A. Chen, Algorithm screening to accelerate discovery of 2D metal-free electrocatalysts for hydrogen evolution reaction, *J. Mater. Chem. A*, 2019, **7**, 19290.

43 S. Y. Lin, Y. Guo, M. L. Xu, J. J. Zhao and Y. W. Liang, A B_2N monolayer: a direct band gap semiconductor with high and highly anisotropic carrier mobility, *Nanoscale*, 2022, **14**, 930–938.

44 X. Y. Zhou, X. F. Chen, C. Z. Shu, Y. Huang, B. B. Xiao, W. T. Zhang and L. L. Wang, Two-Dimensional Boron-Rich Monolayer BxN as High Capacity for Lithium-Ion Batteries: A First-Principles Study, *ACS Appl. Mater. Interfaces*, 2021, **13**, 41169–41181.

45 G. Kresse and J. Furthmuller, Efficient iterative schemes for ab initio total-energy calculations using a plane-wave basis set, *Phys. Rev. B: Condens. Matter Mater. Phys.*, 1996, **54**, 11169–11186.

46 G. Kresse and J. Furthmuller, Efficiency of ab-initio total energy calculations for metals and semiconductors using a plane-wave basis set, *Comput. Mater. Sci.*, 1996, **6**, 15–50.

47 J. P. Perdew and Y. Wang, Accurate and simple analytic representation of the electron-gas correlation energy, *Phys. Rev. B: Condens. Matter Mater. Phys.*, 1992, **45**, 13244–13249.

48 P. E. Blöchl, Projector augmented-wave method, *Phys. Rev. B: Condens. Matter Mater. Phys.*, 1994, **50**, 17953–17979.

49 J. P. Perdew, K. Burke and M. Ernzerhof, Generalized gradient approximation made simple, *Phys. Rev. Lett.*, 1996, **77**, 3865–3868.

50 S. Grimme, S. Ehrlich and L. Goerigk, Effect of the damping function in dispersion corrected density functional theory, *J. Comput. Chem.*, 2011, **32**, 1456–1465.

51 S. Grimme, Accurate description of van der Waals complexes by density functional theory including empirical corrections, *J. Comput. Chem.*, 2004, **25**, 1463–1473.

52 A. Roudgar and A. Groß, Water bilayer on the Pd/Au(111) overlayer system: Coadsorption and electric field effects, *Chem. Phys. Lett.*, 2005, **409**, 157–162.

53 Y. Gohda, S. Schnur and A. Groß, Influence of water on elementary reaction steps in electrocatalysis, *Faraday Discuss.*, 2009, **140**, 233–244.

54 S. Yao, X. Zhang, A. Chen, Z. Zhang, M. Jiao and Z. Zhou, Algorithm screening to accelerate discovery of 2D metal-free electrocatalysts for hydrogen evolution reaction, *J. Mater. Chem. A*, 2019, **7**, 19290–19296.

55 X. Yang, N. Gao, S. Zhou and J. Zhao, MXene nanoribbons as electrocatalysts for the hydrogen evolution reaction with fast kinetics, *Phys. Chem. Chem. Phys.*, 2018, **20**, 19390–19397.

56 W. W. Qian, Z. Chen, J. F. Zhang and L. C. Yin, Monolayer MoSi2N4-x as promising electrocatalyst for hydrogen evolution reaction: A DFT prediction, *J. Mater. Sci. Technol.*, 2022, **99**, 215–222.

57 X. Q. Wan, C. L. Yang, X. H. Li and Y. L. Zhao, Two-dimensional trilayer heterostructures with cascade dual Z-schemes to achieve efficient hydrogen evolution reaction, *J. Mater. Chem. A*, 2024, **12**, 2359–2372.

58 R. Sun, C. L. Yang, M. S. Wang and X. G. Ma, High solar-to-hydrogen efficiency photocatalytic hydrogen evolution reaction with the HfSe2/InSe heterostructure, *J. Power Sources*, 2022, **547**, 232008.

59 J. Greeley, T. F. Jaramillo, J. Bonde, I. Chorkendorff and J. K. Nørskov, Computational high-throughput screening of electrocatalytic materials for hydrogen evolution, *Nat. Mater.*, 2006, **5**, 909–913.

60 Q. K. Yin, C. L. Yang, M. S. Wang and X. G. Ma, Two-dimensional heterostructures of AuSe/SnS for the photo-catalytic hydrogen evolution reaction with a Z-scheme, *J. Mater. Chem. C*, 2021, **9**, 12231.

61 X. Q. Wan, C. L. Yang, X. H. Li, M. S. Wang and X. G. Ma, Insights into Photogenerated Carrier Dynamics and Overall Water Splitting of the CrS3/GeSe Heterostructure, *J. Phys. Chem. Lett.*, 2023, **14**, 9126–9135.

62 J. K. Nørskov, T. Bligaard, A. Logadottir, J. R. Kitchin, J. G. Chen and S. Pandelov, Trends in the Exchange Current for Hydrogen Evolution, *J. Electrochem. Soc*, 2005, **152**, J23–J26.

63 G. Gao and L.-W. Wang, Substantial potential effects on single atom catalysts for the oxygen evolution reaction simulated via a fixed potential method, *J. Catal.*, 2020, **391**, 530–538.

64 Y. Ji, Y. Li, H. Dong, L. Ding and Y. Li, Ruthenium single-atom catalysis for electrocatalytic nitrogen reduction unveiled by grand canonical density functional theory, *J. Mater. Chem. A*, 2020, **8**, 20402–20407.

65 G. Gao, A. P. O'Mullane and A. Du, 2D MXenes: a new family of promising catalysts for the hydrogen evolution reaction, *ACS Catal.*, 2017, **7**, 494–500.

66 Y. Huang, R. J. Nielsen, W. A. Goddard and M. P. Soriaga, The Reaction Mechanism with Free Energy Barriers for Electrochemical Dihydrogen Evolution on MoS2, *J. Am. Chem. Soc.*, 2015, **137**, 6692–6698.